Vortex magnetic induction: Mathematical, geometric and experimental characterization

A. D. Ramirez-Galindo, H. A. Pérez-Olivas, G. Basurto-Islas,
A. Hernández-Rayas, F. González López and T. Cordova-Fraga

División de Ciencias e Ingenierías, Universidad de Guanajuato, Campus León, Loma del Bosque n. 103, Lomas del Campestre, León, Guanajuato, México.

Received 17 February 2023; accepted 27 December 2023

Some current energy transfer modules and magnetic stimulation systems with vortex fields are mostly composed of a Rodin coil. It has been hypothesized that the most significant changes in the biological system stimulated with vortex magnetic fields are related to the type of field lines and its magnetic field gradient. Therefore, to take advantage of its efficiency, it is necessary to characterize the vortex magnetic field produced inside this coil and to define the behavior of the field gradient. The theoretical Biot-Savart law for this coil geometry is discussed in this work, and the magnetic induction lines are characterized. Magnetic field modeling was carried out with the finite element method; the above processes correlated with the register of the magnetic field of the Rodin performed with a three-dimensional magnetometer. Furthermore, the obtained results with Rodin coil stimulation were compared with those obtained with Helmholtz coil stimulation of a similar biological system. The effect is widely evident in the first case.

Keywords: FEM model; magnetic stimulation; simulation; vortex.

DOI: https://doi.org/10.31349/RevMexFis.70.030901

1. Introduction

The generation of magnetic fields at the micro and nanoscale has been employed in a wide variety of applications, including magnetic domains and thermal propagation in thermal insulators [1], the detection of nanoparticle labels in biomaterials [2], high-density image storage on magnetic tapes [3], and some other reports indicating the biological effects of magnetic fields [4-6]. Magnetic stimulation is a noninvasive alternative treatment for different pathologies such as Alzheimer's disease, Parkinson's disease, and depression, among others, which means an advantage over current treatments, such as transcutaneous or deep electrical stimulation, due to the complexity of the application.

The most relevant results in the application of magnetic fields focused on Alzheimer's disease showed the effect on cell proliferation and cytoprotection, demonstrating promising effects under different stimulation conditions [7, 8]. In some studies, the effect of magnetic stimulation has been tested in animal models, indicating an increase in cognitive abilities [9] and memory enhancement [10]. The use of vortex magnetic fields has emerged as an alternative in the study of the effect on biological tissue stimulation, demonstrating the induction of proliferation of cell lines [11] and human lymphocytes [12], as well as the reduction of amyloid beta protein aggregates associated with Alzheimer's disease [13].

An accurate way to estimate the effect of magnetic stimulation involves describing and characterizing the field in three-dimensional space. For this, obtaining a mathematical model of the field generation system is required under predetermined stimulation conditions.

A fundamental calculation in electromagnetism is the magnetic field due to current flow in a wire of finite length using the Biot-Savart law. The calculation is based on considering some crucial limitations for more complex geometries; for example, the filament that acts as a field source and the observation point is located on one of the axes (or parallel to them). However, it is necessary to study the field at an arbitrary point in space due to a segment that is not necessarily located on one of the axes; in that case, the complexity of the calculations is higher.

The magnetic field gradient physically represents the variation in magnitude concerning spatial variables. The change of the function should be considered if a value difference in the direction of interest is known, applying the corresponding vector operation with the nabla operator.

The mathematical modeling, design, and geometric construction of the Rodin coil [14] as a source of the magnetic field in a dodecagon configuration are presented in this manuscript.

The theoretical procedure for the coil geometry is validated with simulation software based on the finite element method, obtaining the quantized spatial distribution of the magnetic field that radiates around.

On the other hand, a three-dimensional magnetic field XYZ scanning system is built with a scanned space of $16 \times 16 \times 8$ cm, performing a position sweep with the triaxial sensor in the space surrounding the Rodin coil.

2. Geometric analysis and mathematical model

For the geometric design of the Rodin coil, the position in the space of the field source is considered, as well as an observa-

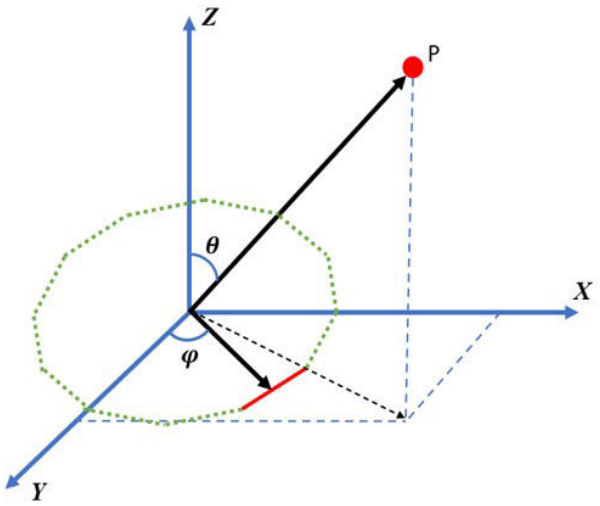

FIGURE 1. The geometric approach of the field source (formed by 12 segments, represented by the dotted line, the mathematical analysis is performed for the individual red segment, superimposing the result for the 12 segments) and the observation point P.

tion point; this approach is shown in Fig. 2. The field source was thought to be a dodecagon in the XY plane.bn

Considering the vectorial approach, the geometric construction is carried out in each segment, resulting in the superposition of the field due to all the segments. Subsequently, two vectors are proposed: the position vector of the observation point $\overrightarrow{r}$ and the position vector of the field source $\overrightarrow{r'}$. The resulting vector of the two vectors $\overrightarrow{R}$ is calculated. Due to how the field is propagated in space, the spherical coordinate system is chosen, starting from cartesian coordinates.

$$\overrightarrow{r} = r\widehat{r}, \tag{1}$$

$$\overrightarrow{r'} = r'\widehat{r}, \tag{2}$$

$$\overrightarrow{R} = (r - r')\widehat{r}. \tag{3}$$

It is relevant to know the vector that represents the trajectory of the segment of the coil through which the current flows. For the case of the Rodin coil, the line differential in spherical coordinates with all its components is considered [15].

$$d\overrightarrow{l} = dr\widehat{r} + rd\theta\widehat{\theta} + r\sin(\theta)d\phi\widehat{\phi}. \tag{4}$$

Therefore, with the geometric design, the substitution is made in the expression of the Biot-Savart law:

$$\overrightarrow{B} = \frac{\mu_0 I}{4\pi}\int \frac{d\overrightarrow{l}\times\overrightarrow{R}}{R^2}. \tag{5}$$

The following expression is obtained by applying the respective vector operations and converting the resulting expression to the cartesian coordinate system.

$$\overrightarrow{B} = \frac{N\mu_0 Ir}{4(r-R)^2}\left[\left(\frac{zx}{ar} - \frac{24y}{a}\right)\widehat{i} + \left(\frac{zy}{ar} - \frac{24x}{a}\right)\widehat{j} - \left(\frac{a}{r}\right)\widehat{k}\right]. \tag{6}$$

Here $r = \sqrt{x^2+y^2+z^2}$, and $a = \sqrt{x^2+y^2}$.

Where N is the number of winding turns, n is the number of sides of the polygon that is formed during the winding process, I is the supply current, and R is the average radius of the polygon opening.

With the potential formulation, the magnetic induction can be expressed by the following expression:

$$\overrightarrow{B} = \nabla \times \overrightarrow{A}, \tag{7}$$

where $\overrightarrow{A}$ is the magnetic vector potential and ∇ is the nabla operator that represents a vector operation related to the variation of any function concerning three spatial variables. This expression represents the calculation of the magnetic field gradient.

3. Simulation by the finite element method

The mathematical model of the Rodin coil is based on the so-called Rodin numerical map, which describes the spiral pattern to produce magnetic field vortices. The configuration involves winding onto a toroid with 36 poles distributed along its median plane. The winding process follows an angular separation of 150° between poles, measured relative to the center of the toroid. For specific purposes, only 12 poles of the 36 proposed are considered, with a separation of 30° between poles. The design of a Rodin coil requires two main variables: the diameter of the aperture generated by the winding around the toroid and the magnitude of the field at the center of the geometry; the other variables needed to build the geometry can be obtained using geometric expressions. The physical parameters of the model are shown in Table I.

TABLE I. List of parameters defined in the mathematical model.

Parameter	Variable	Units
External diameter of the toroid	D	m
Internal diameter of the toroid	d	m
Toroid aperture diameter	$2R_c$	m
Distance from the center of the toroid to the edge	$R_p = \frac{D}{2}$	m
Number of poles	N_{poles}	–
Winding angle between P1, 0, P6	θ_s	rad
Angle between R_p, P1, P6	θ	rad
Angle between R_p and r	γ	rad
Angle between X_{el} and r	β	rad
Distance between points P1 and P6	l	m

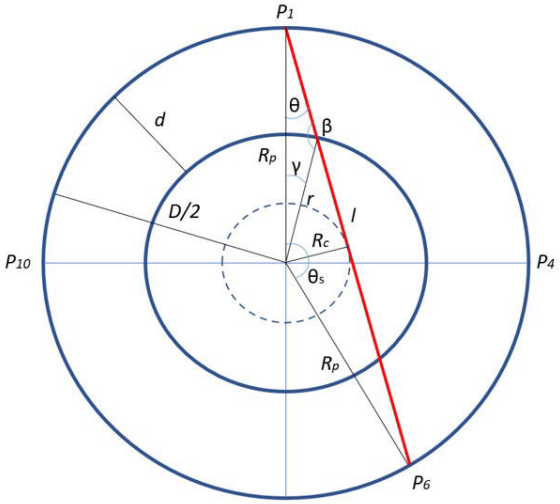

FIGURE 2. Projection in a 2D plane of the winding of a Rodin coil. The red line represents the construction of the first segment of the polygon.

In Fig. 1, the first two points (P1, P6) are used to determine a segment, taking geometric considerations and symmetry into account, and establishing a model.

Given the right triangle formed by the segment R_p, R_c and l/2, the sum of the internal angles (right angle, θ and $\theta_s/2$) is equal to 180°C, with the opening radius and the angle of winding (θ_s) required, the value of the segment R_p can be calculated using the following expression:

$$R_c = R_p \sin(\theta), \tag{8}$$

R_p represents the outer radius of the toroid winding. In the 3D model design, the winding aperture does not change considering the curve of the winding on the toroid, but the change is reflected in the length l, using half of the isosceles triangle to estimate the length of segment l.

$$l = 2R_p \cos(\theta), \tag{9}$$

A Rodin coil model bears the following characteristics:

- External diameter of the toroid: 9.95 cm.
- Aperture diameter: 2.9 cm.
- Number of poles: 12.
- Winding angle: 150°C.

The design of the simplified 3D model was carried out in the Autodesk Inventor software, and later the geometry was imported into the Comsol Multiphysics simulation software, configuring the conditions to the domains that represent the physics in steady state, that is, the excitation current does not vary on time and frequency. The material assigned to the domains for the coil is copper, and the space around the coil is air. The discretization of the domain is generated by dividing the physics into tetrahedral geometric elements. As a result of the simulation, the freedom degrees in this study are 229,522, and an average simulation time is 1 min using an Intel CORE i7 processor.

4. System construction and magnetic field measurement

After the model was validated with the construction of the system and performing a scan of the field lines, an automatic measurement system with a triaxial magnetic field sensor was implemented.

The geometric model used for the simulation by the finite element method to build the stimulation coil is taken as a basis, as well as the typical winding pattern of a Rodin coil, in Fig. 3a), a dodecagon shape is observed within the geometry; Fig. 3b) is illustrated on a plastic toroid where a copper wire is wound into a pattern.

The Rodin stimulation system consists of a frequency generator module (1), which uses a mobile device to select the desired frequency, as shown in Fig. 4. The resulting frequency is sent through an audio interface to the amplifier

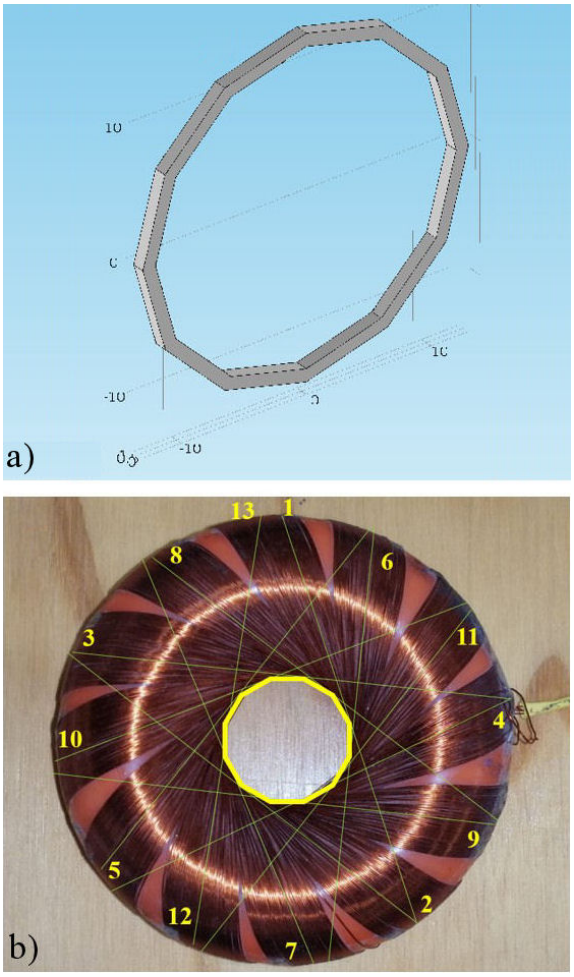

FIGURE 3. a) Simplified model of the geometry used for the simulation by the finite element method. b) Top view of the winding and representation of the winding pattern.

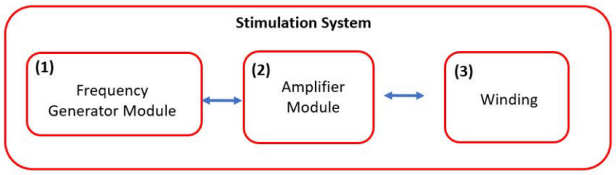

FIGURE 4. Block diagram of the Rodin coil wound pattern stimulation system.

module (2) with a 12 V power supply. Then the amplified signal is delivered to the winding pattern (3) which is made up of two coils connected in series, generating a magnetic field inside the coils. For the mechanical design of an automated XYZ Cartesian table, it is required to implement a methodology integrating mechanical, electrical, and control subsystems.

1. The metallic structure is the central mechanical subsystem of the table; square 54×54 cm PTR (Rectangular Tubular Profile) aluminum profiles were selected, for the columns and beams. The guides are located along the table and where the mobile beam that supports the tool holder moves. Two linear guides are part of this subsystem: a servomotor and an axis aligning the two guides. Two toothed band guides were selected for the linear displacement in this axis, from the movement systems, two stepper motors with a torque capable of moving the metallic assembly can be defined.

2. A programmable ATmega2560 microcontroller was used for electrical subsystems, integrating an H-bridge controller module to activate and deactivate the coils contained in the stepper motor.

3. The control subsystem presents four stages, as shown in Fig. 5. The data entry stage, which is data acquisition of mapping coordinates in two dimensions, defines the instructions in G code for displacement in a cubic area of 21 cm^3. In the pre-processing stage, the activation of the motors is carried out in the movement of the carriages to position the measurement sensor in the volume to be mapped. The processing stage activates the Hall effect sensor and starts the sweep sequence, and finally, in the post-processing stage, the mapped field signals are stored on a microSD.

The three-dimensional magnetic field XYZ scanning system consists of a magnetic field sensor (Melexis MLX90393) with measurement characteristics in the vector X, Y, and Z components, with a measurement range of 5-50 mT and a resolution of up to 0.161 μT [16–19]. The choice of the sensor was based on the ease of configuration for obtaining data, as well as the small size of the integrated circuit, which allows a position sweep with steps of 0.5 cm. Additionally, a Hall effect sensor is effective when measurements on the order of micro and milli Teslas are required.

From the combination of linear movements, complex trajectories can be generated in a three-dimensional space. A

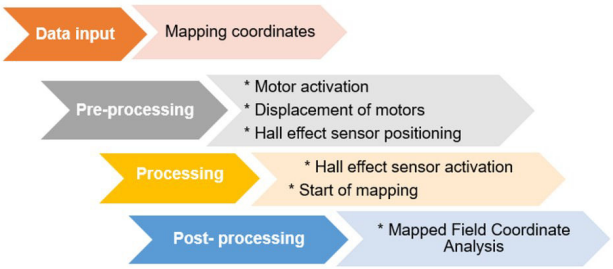

FIGURE 5. Stages of the control subsystem.

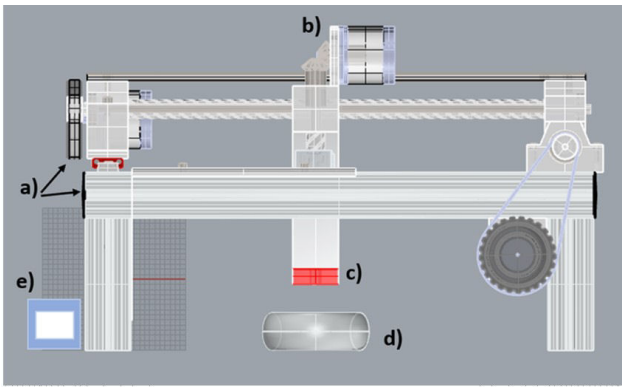

FIGURE 6. Mechanical design of a Cartesian XYZ table, a) Support for motors in XY axes, b) Support for motor in the Z axis, c) Hall effect sensor, d) Rodin coil, and e) Sweep control screen.

Cartesian table's mechanical design, as shown in Fig. 6, includes: a) support for motors in the XY axes; b) support for motors in the axes; c) Hall effect sensor; d) Rodin coil; and e) swept control screen. The obtained data is plotted in three-dimensional space, highlighting the importance of the vector characteristics of the field. At each point in space, the magnetic magnitude of the three components (X, Y, Z) that describe the magnitude of the field is recorded.

5. Results

The importance of characterizing the field generated by the Rodin coil lies in the interest of knowing the effect of vortex magnetic induction in biological applications.

The mathematical modeling resulted in obtaining an expression that describes the behavior of magnetic field vectors in a three-dimensional space produced by a 12-sided regular polygon. It is important to mention that since the model is a mathematical expression dependent on physical variables, there may be indeterminacies when evaluating the expression numerically. Hence, it is necessary to consider limitations in the calculation. However, when comparing the results obtained by plotting this model with the model built in the physics resolution software by the finite element method, it can be observed that there is a similarity in the spatial distribution of the field vectors, as well as in the field magnitude

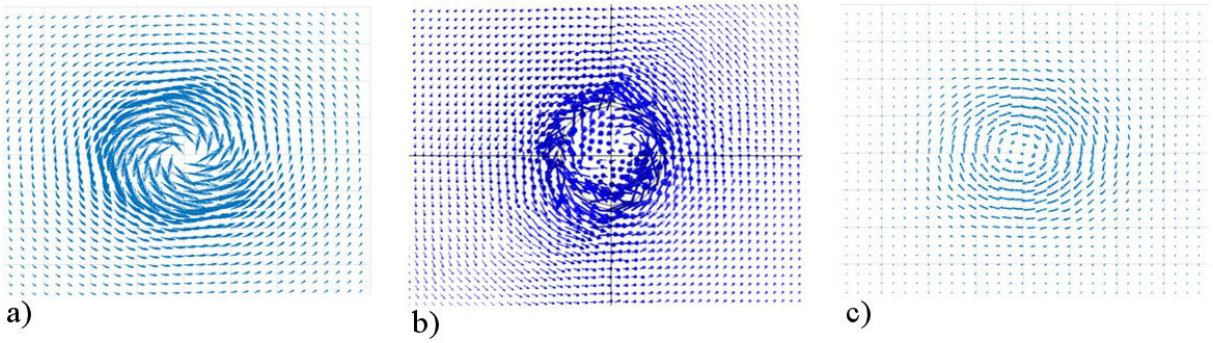

FIGURE 7. 3D graph of the magnetic field vectors at points in the space surrounding the Rodin coil by the models: a) Mathematical, b) geometric (simulation), and c) experimental.

TABLE II. Comparison of the magnitude of the magnetic induction intensity ([mT]) in the developed models.

Electric Current Intensity [A]	Theoretical Value [mT]	Simulated Value [mT]	Experimental Value [mT]
1.60	3.90	4.08	4.13
1.25	3.01	3.00	3.05
0.60	1.30	1.10	1.16

measured at a point, even though a simplified model is simulated in the software due to computational power limitations. This simplification cannot be applied to real life, since the coil construction process follows a pattern determined by the Rodin numerical map and a variation in the winding generates a different geometry and, consequently, a significant difference in the values of the countryside. The construction of an electronic measurement system made it possible to validate the calculated and simulated values of simplified models of the actual geometry at specific points in space.

The characterization of the field based on three models (mathematical model, finite element software model, and experimental model) allows for confirming the vortex nature of the magnetic field generated by the Rodin coil. The distribution of the field in the space surrounding the models is shown in Fig. 7. This magnetic field distribution is helpful for various applications, so knowing its characteristics allows us to take advantage of the potential that a magnetic field represents.

In the graphs comparison, the vortex nature of the field generated by the Rodin coil is verified, and it is observed that there is a similarity between the three stages of the characterization. Table II shows a comparison of the value of the magnitude of the magnetic field at the center of the geometry.

6. Discussion

Gradients are an essential factor for the survival of organisms in their environment; for example, cells present movement according to gradients of different physical variables, such as temperature, gravitational forces, chemical concentrations, and light or electromagnetic fields, to be in an optimal environment [20, 21]. The importance of field gradients has been demonstrated in various research papers where the behavior of cell groups in the presence of a high-magnitude gradient magnetic field is studied [22].

Various stimulation studies using the Rodin coil present results that demonstrate an increase in cell viability and prevent the aggregation of the amyloid beta protein [13] or modification in protein expression [23]; In both study cases, the stimulation conditions are similar: field strengths between $1-2$ mT, frequency ranges between $50-75$ Hz. However, they differ in the Rodin coil geometry, indicating that the gradient differs between both studies.

In general, if the effect of the Rodin coil is compared with some other geometry that generates homogeneous fields (such as the case of the Helmholtz coil), it is significantly increased by up to 60% [24].

The comparison between both cases again highlights the importance of characterizing the field generated by the coil geometry, to correlate the effect obtained with the physical and operating characteristics of the coil.

The hypothesis underlying the present work is that the increase in any tested effect produced by Rodin coil compared to the Helmholtz coil is because the magnetic field gradient in the case of the Rodin coil is significantly larger than in the case of the Helmholtz coil.

The effect of the gradient can be explained by knowing that a charged particle moves in the presence of a magnetic field. This principle is applied in the biological field because the movement of charges (ions) within the cell along with the surrounding environment produces different effects related to its specific function. Therefore, the magnetic field with a high gradient applied to a cell culture magnifies the effect produced under homogeneous stimulation conditions.

In the case of the geometry proposed in this paper, when graphing the results, they confirm the vortex nature of the magnetic field, whose effect could be compared with those reported in research articles.

7. Conclusions

This is the first research work that presents a complete characterization of the magnetic field intending to estimate the effect in the biological assay. The mathematical modeling of the Rodin coil through the expression of the Biot-Savart law is a core part of the work since the geometric considerations are the basis for the proposal of the model used for the simulation by the finite element method.

The finite element model simplifies the actual geometry, the intention being to prove that the winding trace outside the dodecagon does not contribute significantly to the magnetic field. This simplification consumes fewer computational resources than the complete geometry; however, the results are comparable with those obtained in the mathematical model.

The two models (theoretical and simulated) are not realistic since they only represent the polygon as a field source; despite this, the results obtained are close to the field values measured by the three-dimensional mapping system and the magnetic field sensor.

The work can be a guideline for estimating the effect of magnetic stimulation in cell culture or animal models since the field's spatial distribution and direction at any point in space are known in detail.

Acknowledgments

This work was partially supported by University of Guanajuato under "Convocatoria Institucional de Investigación Científica (CIIC) 2024" and CONAHCYT Scholarship CVU: 1009300.

Conflict of interest

The authors have no conflicts to disclose.

Author's contribution

All authors contributed equally to this work.

1. W. Jiang *et al.,* Direct imaging of thermally driven domain wall motion in magnetic insulators, Physical review letters **110** (2013) 177202, https://doi.org/10.1103/PhysRevLett.110.177202.
2. S. Cardoso *et al.*, Challenges and trends in magnetic sensor integration with microfluidics for biomedical applications, Journal of Physics D: Applied Physics **50** (2017) 213001, https://doi.org/10.1088/1361-6463/aa66ec.
3. S. Porthun, L. Abelmann, and C. Lodder, Magnetic force microscopy of thin film media for high density magnetic recording, Journal of magnetism and magnetic materials **182** (1998) 238, https://doi.org/10.1016/S0304-8853(97)01010-X.
4. E. Foroozandeh, P. Derakhshan-Barjoei, and M. Jadidi, Toxic effects of 50 Hz electromagnetic field on memory consolidation in male and female mice, Toxicology and industrial health **29** (2013) 293, https://doi.org/10.1177/0748233711433931.
5. I.-F. Chang and H.-Y. Hsiao, Induction of RhoGAP and pathological changes characteristic of Alzheimer's disease by UAHFEMF discharge in rat brain, Current Alzheimer Research **2** (2005) 559, https://doi.org/10.2174/156720505774932269.
6. F. Teimori *et al.*, The effects of 30 mT electromagnetic fields on hippocampus cells of rats, Surgical Neurology International **7** (2016), https://doi.org/10.4103/2152-7806.185006.
7. N. Marchesi *et al.,* Autophagy is modulated in human neuroblastoma cells through direct exposition to low frequency electromagnetic fields, Journal of cellular physiology **229** (2014) 1776, https://doi.org/10.1002/jcp.24631.
8. C. Osera *et al.,* Pre-exposure of neuroblastoma cell line to pulsed electromagnetic field prevents H2O2-induced ROS production by increasing MnSOD activity, *Bioelectromagnetics* **36** (2015) 219, https://doi.org/10.1002/bem.21900.
9. G. W. Arendash *et al.,* Electromagnetic field treatment protects against and reverses cognitive impairment in Alzheimer's disease mice, Journal of Alzheimer's disease **19** (2010) 191, https://doi.org/10.3233/JAD-2010-1228.
10. G. W. Arendash *et al.,* Electromagnetic treatment to old Alzheimer's mice reverses β-amyloid deposition, modifies cerebral blood flow, and provides selected cognitive benefit, PLoS One **7** (2012) e35751, https://doi.org/10.1371/journal.pone.0035751.
11. T. Cordova-Fraga *et al.*, Increasing survival study of kidney HEK-293T cells in magnetic field vortices and nano-fluid, IJEIT **4** (2014) 222
12. F. P. Perez *et al.*, Electromagnetic field therapy delays cellular senescence and death by enhancement of the heat shock response, Experimental gerontology **43** (2008) 307, https://doi.org/10.1016/j.exger.2008.01.004.
13. A. Maldonado-Moreles *et al.*, Low frequency vortex magnetic field reduces amyloid β aggregation, increase cell viability and protect from amyloid β toxicity, Electromagnetic Biology and Medicine **40** (2021) 191, https://doi.org/10.1080/15368378.2020.1830288.
14. M. Rodin and G. Volk, The rodin number map and rodin coil, Proceedings of the NPA **7** (2010) 437
15. D. J. Griffiths, Introduction to electrodynamics, 2nd ed. (Prentice Hall, Englewood Cliffs, NJ, 1989), pp. 331-334.
16. MLX90393 Triaxis Micropower Magnetometer - Melexis Mouser., https://www.mouser.mx.
17. 2.8 TFT Touch Shield for Arduino with Resistive Touch Screen, https://www.adafruit.com/product/1651.
18. L298N: módulo para controlar motores para Arduino — Hardware libre., https://www.hwlibre.com/l298n/.

19. Arduino - Products., https://www.arduino.cc.

20. V. Zablotskii, T. Polyakova, and A. Dejneka, Cells in the nonuniform magnetic world: how cells respond to high-gradient magnetic fields, *BioEssays* **40** (2018) 1800017, https://doi.org/10.1002/bies.201800017.

21. V. Zablotskii *et al.*, How a high-gradient magnetic field could affect cell life, *Scientific reports* **6** (2016) 1, https://doi.org/10.1038/srep37407.

22. V. Zablotskii *et al.*, Life on magnets: stem cell networking on micro-magnet arrays, *PloS one* **8** (2013) e70416, https://doi.org/10.1371/journal.pone.0070416.

23. D. I. Aparicio-Bautista *et al.*, An Extremely Low-Frequency Vortex Magnetic Field Modifies Protein Expression, Rearranges the Cytoskeleton, and Induces Apoptosis of a Human Neuroblastoma Cell Line, *Bioelectromagnetics* **43** (2022) 225, https://doi.org/10.1002/bem.22400.

24. J. Saikia *et al.*, Electric field disruption of amyloid aggregation: Potential noninvasive therapy for Alzheimer's disease, *ACS chemical neuroscience* **10** (2019) 2250, https://doi.org/10.1021/acschemneuro.8b00490.